Effect of high-temperature buffer thickness on quality of AlN epilayer grown on sapphire substrate by metalorganic chemical vapor deposition*

Liu Bo(刘 波)[a)†], Zhang Sen(张 森)[b)], Yin Jia-Yun(尹甲运)[a)], Zhang Xiong-Wen(张雄文)[a)], Dun Shao-Bo(敦少博)[a)], Feng Zhi-Hong(冯志红)[a)], and Cai Shu-Jun(蔡树军)[a)]

[a)] *Science and Technology on ASIC Laboratory, Hebei Semiconductor Research Institute, Shijiazhuang* 050051, *China*
[b)] *School of Physical and Mathematical Sciences, Nanyang Technology University, Singapore* 637371, *Singapore*

(Received 10 October 2012; revised manuscript received 25 October 2012)

The effect of an initially grown high-temperature AlN buffer (HT-AlN) layer's thickness on the quality of an AlN epilayer grown on sapphire substrate by metalorganic chemical vapor deposition (MOCVD) in a two-step growth process is investigated. The characteristics of AlN epilayers are analyzed by using triple-axis crystal X-ray diffraction (XRD) and atomic force microscopy (AFM). It is shown that the crystal quality of the AlN epilayer is closely related to its correlation length. The correlation length is determined by the thickness of the initially grown HT-AlN buffer layer. We find that the optimal HT-AlN buffer thickness for obtaining a high-quality AlN epilayer grown on sapphire substrate is about 20 nm.

Keywords: AlN epilayer, high-temperature (HT) buffer, atomic force microscopy (AFM), dislocation

PACS: 71.55.Eq, 78.66.Fd, 73.21.Ac **DOI:** 10.1088/1674-1056/22/5/057105

1. Introduction

Recently, AlN and AlGaN-based ultraviolet (UV) emitters, such as UV and deep-UV light-emitting diodes (LEDs) and laser diodes (LDs), have been applied in medicine and for white-light illumination.[1] However, the performance of the current nitride-based UV emitters is impeded by threading dislocations (TDs) that originate from the substrate since no substrate material is suitably lattice-matched for growing any nitrides.[2,3] Sapphire is preferred as the substrate for the fabrication of UV emitter device structures because of its low cost and its transparency to UV light. Hence, it is very important to control the crystal quality of AlN layers on sapphire substrates.

Usually, AlN layers on sapphire substrate are grown by using a low-temperature AlN (LT-AlN) buffer layer, but some groups have reported growth of high-quality AlN on sapphire by using a high-temperature (HT)-AlN buffer layer.[4,5] Moreover, the crystal quality of the AlN epilayer is very sensitive to the initial growth state.[6–8] Motivated by this, we introduce HT-AlN layers as buffer layers and investigate their effect on the structural features. To avoid a strong vapor-phase reaction between trimethylaluminum (TMA) and ammonia (NH_3), a low-pressure flow-modulated (FM) metalorganic chemical vapor deposition (MOCVD) method is adopted for the consequent AlN epilayer growth. In order to optimize the HT-AlN buffer layer for obtaining high-quality FM-AlN epilayer, the influence of the thickness of the HT-AlN buffer layer on the quality of the FM-AlN epilayer is studied in detail.

2. Experiments

AlN epilayer growth was performed on *c*-plane sapphire substrates by MOCVD. Nitrogen and hydrogen were used as carrier gases to transport the TMA and NH_3 into the reactor through separate gas channels. The initial HT-AlN buffers were grown under TMA and NH_3 flows, and opened at the same time with various thicknesses of 10 nm, 20 nm, 30 nm, and 50 nm corresponding to samples A, B, C, and D, respectively. Following the initial buffer layer growth, FM-MOCVD growth was continued at the same temperature as shown in Fig. 1. The FM-MOCVD growth time for all the samples was 1 h, and the thickness was about 200 nm. The atomic force microscopy (AFM) was used to characterize the surface morphology over an area of 5 μm×5 μm in tapping mode. The correlation length of the sample was estimated based on the AFM measurement. The structural characteristics were investigated by X-ray diffraction (XRD) rocking curves for reflexes which were sensitive to screw and mixed dislocations (002) and to all dislocations (102).

3. Results and discussion

3.1. XRD analysis

Rocking curves of ω scans of the (002) and (102) reflections were measured, and representative results for a 200-nm AlN epilayer are illustrated in the inset of Fig. 2. The

*Project supported by the National Natural Science Foundation of China (Grant No. 60876009).
†Corresponding author. E-mail: liub.hsri@foxmail.com
© 2013 Chinese Physical Society and IOP Publishing Ltd

main plot of Fig. 2 shows the full width at half maximum (FWHM) of rocking curves of ω scans of the (002) and (102) reflections as a function of the HT-AlN buffer layer thickness. The FWHM of the (002) rocking curve moderately decreases with increasing the thickness. The FWHM value of the (102) rocking curve with 20-nm HT-AlN buffer layer is smaller than that of samples A, C, and D. The minimum FWHM value (about 1113 arcsec) was observed in sample B with an HT buffer thickness of about 20 nm.

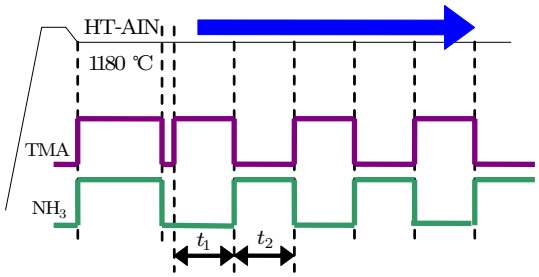


Fig. 1. (color online) Wafer temperature and the flow sequence of TMA and NH_3 for thermal cleaning, HT-AlN layer growth, and FM-MOCVD growth ($t_1 = 3$ s, $t_2 = 2$ s).

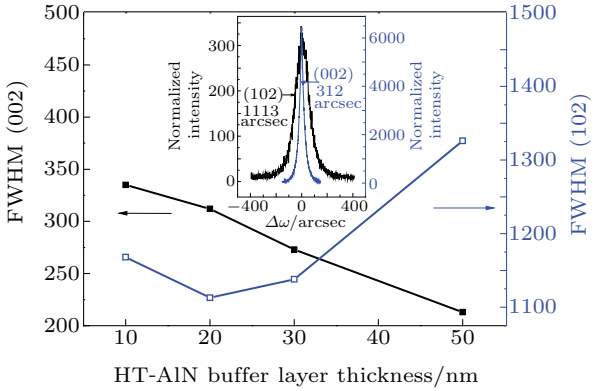


Fig. 2. (color online) HT-AlN thickness dependence of FWHM of (002) and (102) rocking curves of FM-AlN epilayers. XRD rocking curves of the (002) and (102) planes of a 3-min HT-AlN epilayer are shown in the inset.

We used the FWHM of the (002) reflection to estimate the tilt angle β_{tilt}.[9] The twist angle was estimated using the method outlined previously by Lee *et al.*[10]

$$\Delta\theta = \left[(\beta_{\text{tilt}}\cos\varphi)^2 + (\beta_{\text{twist}}\sin\varphi)^2\right]^{1/2}, \tag{1}$$

where β_{tilt} and β_{twist} are the tilt and twist spreads, respectively, and φ is the angle between the reciprocal lattice vector and the (001) surface normal.

The tilt and twist are related to threading dislocations with screw components (screw and/or mixed TDs) and edge components (edge and/or mixed TDs), respectively. The density of screw TDs (N_{s}) and of edge TDs (N_{E}) are then estimated using the classical formulas[11]

$$N_{\text{s}} = \frac{\beta_{\text{tilt}}^2}{4.35|b_{\text{s}}|^2}, \tag{2}$$

$$N_{\text{E}} = \frac{\beta_{\text{edge}}^2}{4.35|b_{\text{E}}|^2}, \tag{3}$$

where b_{s} and b_{E} are the Burgers vector of screw-type TDs ($b_{\text{s}} = 0.4982$ nm) and the Burgers vector of edge-type TDs ($b_{\text{E}} = 0.3112$ nm), respectively.

For the densities of TDs with edge and screw components as a function of the HT-AlN buffer layer thickness, see Table 1 for details. The densities of TDs with edge components are two orders of magnitude higher than those of TDs with screw components, indicating that TDs with edge components are by far the main type formed in the AlN epilayer. The densities of the TDs with screw components decreased as the HT-AlN buffer layer thickness increased. However, the density of TDs with edge components is minimized with a 20-nm HT-AlN buffer layer. Our results suggest that sample B with its 20-nm HT-AlN buffer layer has a lower threading dislocation density and better crystal quality than all the others.

Table 1. Buffer layer thicknesses and structures of all samples, including the screw-type TDs, the edge-type TDs, and the correlation length.

Sample	Buffer thickness/nm	Screw-type TDs/cm^{-2}	Edge-type TDs/cm^{-2}	Correlation length/μm
A	10	2.4459×10^{8}	1.5539×10^{10}	0.30
B	20	2.1215×10^{8}	1.4139×10^{10}	0.32
C	30	1.6243×10^{8}	1.4953×10^{10}	0.27
D	50	9.887×10^{7}	2.0655×10^{10}	0.24

3.2. AFM analysis

Figure 3 shows the surface morphology of all the AlN epilayer samples grown on the HT-AlN buffer layers of various thicknesses. We can determine the correlation lengths (ξ) of the samples using their power spectral density (PSD), and a Fourier transform of the surface height. A suitable model for the PSD of a self-affine surface is given by[12]

$$\text{PSD}(f) = \frac{4\pi\alpha w^2\xi^2}{(1+\xi^2 f^2)^{1+\alpha}}. \tag{4}$$

Here, α is the roughness exponent, which describes how wiggly the local surface is, w is the interface-wide or root-mean-square roughness, f is the spatial frequency, and ξ is the correlation length.[13] The constants in the formula are then determined by a least squares minimization for all the length scales covered by the AFM measurements.

Figure 4 shows that the PSD exhibits two distinct regions: (i) a plateau PSD at low spatial frequencies denoting an absence of nonlocal correlations along the line scans; (ii) a frequency-dependent decaying branch. The steeper portion of the latter is taken as the self-affine range, while the high-frequency range with smaller slope is discarded since it is more affected by noise and aliasing. The range of the intersection between the self-affine branch and the plateau defines the inverse of the correlation length, and the correlation length is proportional to the effective radius of the domain. This framework allows one to estimate the average domain size independently on an arbitrary statistical basis.[14]

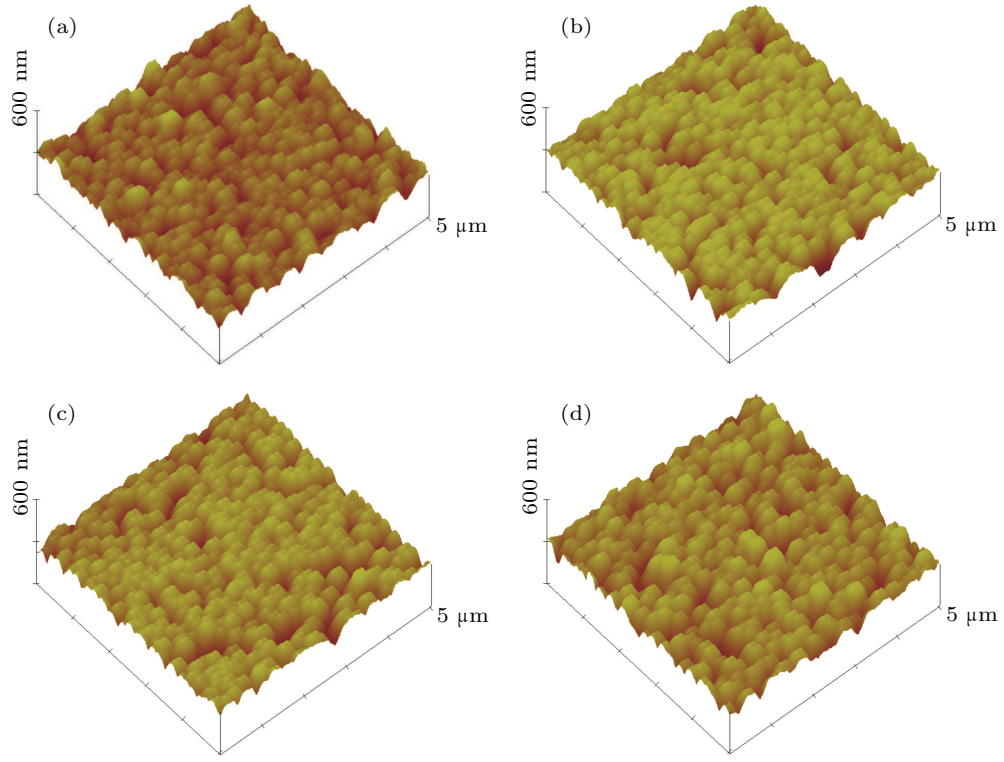


Fig. 3. (color online) The dependence of surface morphology on the buffer thickness of (a) sample A, (b) sample B, (c) sample C, and (d) sample D.

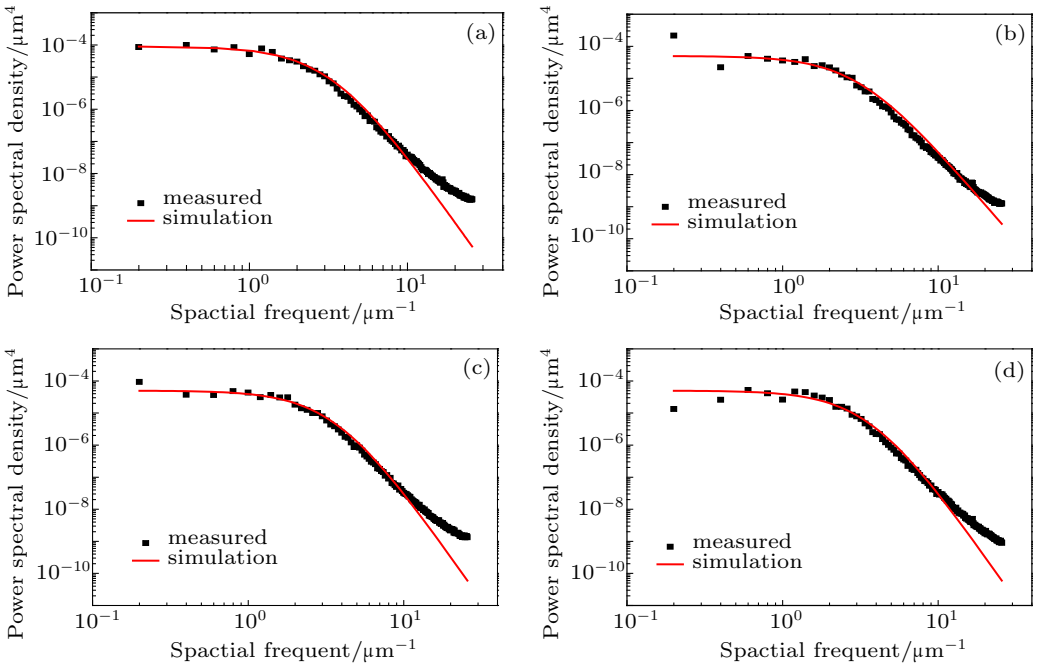


Fig. 4. (color online) The dependence of correlation length on the buffer thickness. (a) sample A, (b) sample B, (c) sample C, and (d) sample D.

We investigate the evolution of the correlation length with the thickness of the HT-AlN buffer layer. The correlation length is a function of the HT-AlN buffer layer thickness, as listed in Table 1. The correlation lengths are maximized for the 20-nm HT-AlN buffer layer, which means that it has the largest grains. Imura *et al.* suggests that most of the dislocations at grain boundaries were determined to be edge-type.[15,16] The mechanism is that three-dimensional grain islands are deposited during the initial stage of the growth, and subsequently, smaller grains are incorporated into bigger grains resulting in much larger grains. Simultaneously, the edge dislocations caused by the grain boundaries come into being dur-

ing the incorporation process of grains. As the HT-AlN buffer layer's thickness increases, it has a larger grain size and higher quality. As a result, the screw dislocations become fewer. The distance is made smaller by increasing the grain size. Thus, we can attribute the decreased density of TDs to the increased grain size.

3.3. Discussion of growth process

We have shown that sample B has the best quality, implying that the quality of the FM-AlN epilayer is closely related to the thickness of the HT-AlN buffer layer. As the thickness of the HT-AlN buffer layer increases, its grain size also increases accordingly within a certain range of thickness.[7] Because the FM-AlN epilayer islands in the initial growth stage will coalesce quickly if the HT-AlN buffer layer has a small grain size and high nuclei density, a lot of the dislocations that form in it will extend through the FM-AlN epilayer, leading to lower quality.[17] Of course, when the thickness of the HT-AlN buffer layer exceeds a certain value, the HT-AlN buffer layer grain size is too large and the nuclei density is too low. Hence, the lateral growth and coalescence of the FM-AlN epilayer islands decreases, leading to bad quality of the AlN epilayer. As a result, there is an optimal thickness for the initial HT-AlN buffer layer which produces large lateral grain size and low nucleation density, promoting the lateral growth and coalescence of the FM-AlN epilayer islands.

4. Summary

We have grown FM-AlN epilayers on the sapphire substrate, using an HT-AlN as a buffer, with MOCVD. Based on the experimental results above, it is found that a 20-nm thick initial HT-AlN buffer layer is optimal for a high-quality AlN epilayer. In addition, the TDs are correlated with the correlation length of the AlN epilayers. The quality of the FM-AlN epilayer strongly depends on the grain size and nuclei density of the HT-AlN buffer layer.

References

[1] Li D B, Hu W G, Miyake H, Hiramatsu K and Song H 2010 *Chin. Phys. B* **19** 127801

[2] Speck J S and Rosner S J 1999 *Physica B* **273** 24

[3] Ye H, Lu P F, Yu Z Y, Yao W J, Chen Z H, Jia B Y and Liu Y M 2010 *Chin. Phys. B* **19** 047302

[4] Paduano Q S, Weyburne D W, Jasinski J and Liliental-Weber Z 2004 *J. Cryst. Growth* **261** 259

[5] Takeuchi M, Shimizu H, Kajitani R, Kawasaki K, Kumagai Y, Koukitu A and Aoyagi Y 2007 *J. Cryst. Growth* **298** 336

[6] Chen G F, Yang H, Wu Y X, Zhu J J, Zhang S M, Tiang D S, Liu Z S, Zhao D G, Wang H and Wang Y T 2010 *Chin. Phys. B* **19** 036801

[7] Taniyasu Y, Kasu M and Makimoto T 2007 *J. Cryst. Growth* **298** 310

[8] Ren F, Hao Z B, Hu J N, Zhang C and Luo Y 2010 *Chin. Phys. B* **19** 117101

[9] Pantha B N, Dahal R, Nakarmi M L, Nepal N, Li J, Lin J Y, Jiang H X, Paduano Q S and Weyburne D 2007 *Appl. Phys. Lett.* **90** 241101

[10] Lee S R, West A M, Allerman A A, Waldrip K E, Follstaedt D M, Provencio P P, Koleske D D and Abernathy C R 2005 *Appl. Phys. Lett.* **86** 241904

[11] Dunn C G and Koch E F 1957 *Acta Metall.* **5** 548

[12] Zhao Y P, Wang G C and Lu T M 2001 *Characterization of Amorphous and Crystalline Rough Surface: Principles and Applications* (New York: Academic Press)

[13] Pelliccione M, Karrbacak T, Gairre C, Wang G C and Lu T M 2006 *Phys. Rev. B* **74** 125420

[14] Biscarini F, Samori P, Greco O and Zamboni R 1997 *Phys. Rev. Lett.* **78** 2389

[15] Imura M, Nakano K, Fujimoto N, Okada N, Balakrishnan K, Iwaya M, Kamiyama S, Amano H, Akasaki I, Noro T, Takagi T and Bandoh A 2007 *Jpn. J. Appl. Phys.* **46** 1458

[16] Imura M, Sugimura H, Okada N, Iwaya M, Kamiyama S, Amano H, Akasaki I and Bando A 2008 *Phys. Stat. Sol. (c)* **5** 1582

[17] Zhao D G, Zhu J J, Liu Z S, Zhang S M, Yang H and Jiang D S 2004 *Appl. Phys. Lett.* **85** 1499